SCIENTIFIC REP⚙RTS

Lowering N$_2$O emissions from soils using eucalypt biochar: the importance of redox reactions

P Quin[1,2,*], S Joseph[3,6,7,*], O Husson[4], S Donne[6], D Mitchell[5], P Munroe[3], D Phelan[8], A Cowie[9] & L Van Zwieten[1,2,10]

Agricultural soils are the primary anthropogenic source of atmospheric nitrous oxide (N$_2$O), contributing to global warming and depletion of stratospheric ozone. Biochar addition has shown potential to lower soil N$_2$O emission, with the mechanisms remaining unclear. We incubated eucalypt biochar (550 °C) – 0, 1 and 5% (w/w) in Ferralsol at 3 water regimes (12, 39 and 54% WFPS) – in a soil column, following gamma irradiation. After N$_2$O was injected at the base of the soil column, in the 0% biochar control 100% of expected injected N$_2$O was released into headspace, declining to 67% in the 5% amendment. In a 100% biochar column at 6% WFPS, only 16% of the expected N$_2$O was observed. X-ray photoelectron spectroscopy identified changes in surface functional groups suggesting interactions between N$_2$O and the biochar surfaces. We have shown increases in -O-C $=$ N /pyridine pyrrole/NH$_3$, suggesting reactions between N$_2$O and the carbon (C) matrix upon exposure to N$_2$O. With increasing rates of biochar application, higher pH adjusted redox potentials were observed at the lower water contents. Evidence suggests that biochar has taken part in redox reactions reducing N$_2$O to dinitrogen (N$_2$), in addition to adsorption of N$_2$O.

It is well established that soils are the dominant source of atmospheric nitrous oxide (N$_2$O), though a full understanding of the complex biotic and abiotic factors governing N$_2$O production and consumption remains to be achieved[1–3]. Amendment of soil with biochar can lead to a reduction of N$_2$O emissions, though under some circumstances biochar amendment has resulted in an increase in N$_2$O emissions[4,5]. A review of literature published from 2007 to 2013 found that biochar reduced soil N$_2$O emissions by a mean $54 \pm 6\%$ (95% confidence interval)[6]. Herbaceous- and wood-based biochars were most effective in reducing emissions, while the mean effect of those made from manure was negligible. Cayuela, Jeffery[7] found that the biochars with a molar H:C$_{org}$ (organic C) ratio of <0.3, indicative of a high degree of aromatic condensation, were more effective in lowering N$_2$O emissions than those with a molar H:C$_{org}$ ratio of >0.5. A study by Lin, Spokas[8] found that biochar application reduced N$_2$O production in three soils, apparently through the reaction of the biochar with various N forms (nitrate, nitrite, or N$_2$O) and

[1]University of New England, Armidale, NSW 2351, Australia. [2]Wollongbar Primary Industries Institute, NSW Department of Primary Industries, 1243 Bruxner Highway, Wollongbar, NSW 2477, Australia. [3]School of Materials Science and Engineering, University of New South Wales, NSW 2052, Australia. [4]CIRAD, UPR AIDA, TAB 115/02 Avenue Agropolis 34398 Montpellier Cedex 5, France and AfricaRice Centre, 01 BP 2031 Cotonou, Bénin. [5]Electron Microscopy Center, AIIM, University of Wollongong, Wollongong NSW, 2522, Australia. [6]Discipline of Chemistry, University of Newcastle, Callaghan NSW 2308, Australia. [7]Department of Physics and Institute for Superconducting and Electronic Materials, University of Wollongong, Wollongong NSW, 2522, Australia. [8]Electron Microscope and X-Ray Unit, University of Newcastle, Callaghan NSW 2308, Australia. [9]NSW Department of Primary Industries, University of New England, Armidale, NSW 2351, Australia. [10]Southern Cross Plant Science, Southern Cross University, Military Road, East Lismore NSW 2480, Australia. *These authors contributed equally to this work. Correspondence and requests for materials should be addressed to L.V.Z. (email: lukas.van.zwieten@dpi.nsw.gov.au)

% biochar (w/w soil)	Mean WFPS (%)				
	L (12)	M (39)	H (54)	3	6
			$\Delta N_2O/inj.N_2O$ (mol/mol)		
0	0.958 (0.085)	1.020 (0.026)	1.025 (0.115)		
1	0.837 (0.054)	0.970 (0.070)	0.914 (0.040)		
5	0.614 (0.081)	0.772 (0.088)	0.652 (0.029)		
100					0.161 (0.012)
Acid-washed sand				1.056 (0.113)	

Table 1. The nett increase in total N_2O content in column air and water relative to N_2O injected, measured at tmax: 300 minutes for acid-washed sand, 100% biochar and 12% WFPS; 360 minutes for 39 and 54% WFPS (s.e.m. in parentheses, $n = 3$).

possibly catalytic involvement of iron (Fe). They concluded that biochar reduced N_2O production in these soils through abiotic (chemodenitrification) mechanisms, and hypothesised that Fe-rich biochar can stimulate the abiotic transformation of nitrate/nitrite/N_2O to N_2[8]. Others have also proposed that Fe(II), and perhaps manganese (Mn)(II), play a key role as a catalyst in the abiotic reduction of nitrate (NO_3^-) in soils[9]. The variability in response to biochar amendment is well recognised, as are the considerable knowledge gaps that exist in understanding the precise mechanisms through which biochar influences soil nitrogen (N) transformations[4–6,10,11].

Diffusion of N_2O through soil is influenced by soil structural characteristics and moisture content. Soil water impedes gas diffusion and the high water solubility of N_2O may play a significant role in retarding its movement in the soil[3,12]. Biochar application can alter soil structure and thus affect soil functions, enhancing porosity and pore connectivity[13], water retention, air-filled porosity and gas transport[14]. While biochar is found to affect the N-cycling microbial community, with consequential impacts on microbial N_2O production[15], it is also suggested that abiotic factors, specifically adsorption or redox reactions on biochar surfaces, may influence N_2O emissions[16,17]. Biochar has considerable aromatic C content which, in spite of its high stability, has redox activity and mainly functions as a reducing agent[16]. Cayuela, Sánchez-Monedero[18] propose that biochar can act as an "electron shuttle" and Klüpfel, Keiluweit[19] found biochars to be redox-active, reversibly accepting and donating up to 2 mmol electrons per gram of biochar. Those produced at highest treatment temperatures (HTTs) of 400–700 °C showing greater activity than those of lower HTTs. It has been noted that Fe minerals may be influential in some of these redox reactions[16,20] and Melton, Swanner[21] observed that discerning whether biotic or abiotic processes control Fe redox chemistry is a major challenge.

Nitrous oxide was injected into columns containing soil/biochar mixes, 100% biochar and sterilised sand (as a system control) to examine the effect of both water content and biochar amendment on diffusion of N_2O gas and to determine the importance of adsorption and redox reactions.

Results

Analysis of N_2O data. For each of the 0, 1 and 5% biochar additions to soil, water-filled pore space (WFPS) values of 12 (0.48), 39 (0.47) and 54 (0.50) % were established, hereafter termed low (L), medium (M) and high (H) WFPS (standard error of the mean (s.e.m.) in parentheses, $n = 3$). Moisture contents of the 100% biochar (BC100%) and sand were estimated to be 6 and 3% WFPS respectively. At the end of the sampling periods (tmax) the change in estimated total quantity of N_2O in air-filled pore space (AFPS) and headspace and dissolved N_2O in WFPS, divided by the estimated quantity of N_2O injected ($\Delta N_2O/inj.N_2O$) for all 0% biochar and acid-washed sand treatments was close to unity (Table 1). Treatments of 1 and 5% biochar had mean values (across all WFPS) of $\Delta N_2O/inj.N_2O$ at tmax of 0.91 and 0.67 respectively. This suggested that some injected N_2O was intercepted by these treatments. Treatments were injected with a mean of 22.2 nmol N_2O (s.e.m. = 1.23 nmol, $n = 6$). When compared with the mean N_2O intercepted by 0% biochar treatments (-25 pmol), the 1 and 5% biochar treatments significantly lowered N_2O emitted, by 2.14 and 7.97 nmol respectively ($p = 0.0094$ and $p = 5.6 \times 10^{-8}$). Although there were differences in $\Delta N_2O/inj.N_2O$ at tmax between treatments of differing mean WFPS at the same biochar content (Table 1), only that between the 39 and 54% WFPS treatments with 5% biochar was significant ($p = 0.018$). For the BC100% treatments, $\Delta N_2O/inj.N_2O$ at tmax was only 0.16 (Table 1). The apparent loss of N_2O within the sampling periods for any treatments containing biochar suggests that some of this gas might have been adsorbed, at least temporarily, or decomposed. Figure 1 shows the mean change in headspace N_2O (injected mol $N_2O)^{-1}$ for each treatment. For soil/biochar columns the associated (Fig. 1) caption includes the significance of differences at tmax between treatments of 0, 1 and 5% biochar, based on both headspace N_2O (injected mol $N_2O)^{-1}$ and estimated $\Delta N_2O/inj.N_2O$. Estimated from headspace N_2O concentration ([N_2O]) at tmax, the mean unaccounted N_2O from headspace and AFPS (injected $N_2O)^{-1}$ (i.e. N_2O injected that was 'missing' from the combined volume of headspace and estimated
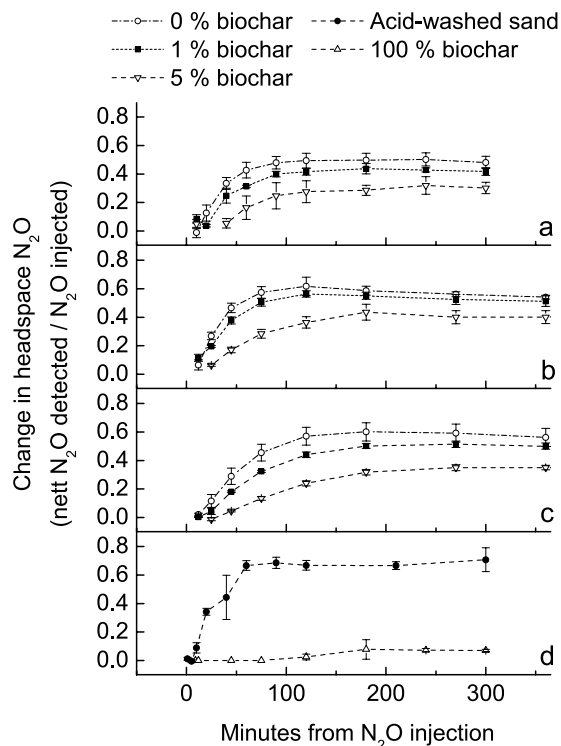
2

Figure 1. The change in mean headspace N_2O (injected $N_2O)^{-1}$ for mean soil water contents of, (**a**) 12% WFPS; (**b**) 39% WFPS; (**c**) 54% WFPS; and also, (**d**) 100% biochar and acid-washed sand (error bars represent ± s.e.m., $n = 3$). At tmax for 12% WFPS the significance of difference in mean nett headspace N_2O (injected $N_2O)^{-1}$ between 0 and 1%, 0 and 5% and 1 and 5% biochar was $p = 0.10$, 0.0058 and 0.018 respectively. For 39% WFPS the corresponding values were $p = 0.31$, 0.0054 and 0.016, and for 54% WFPS were $p = 0.020$, 0.00022 and 0.00079. Accounting for N_2O in WFPS and AFPS, at tmax for 12% WFPS the significance of difference in mean nett (column) total N_2O content (injected $N_2O)^{-1}$ between 0 and 1%, 0 and 5% and 1 and 5% biochar was $p = 0.12$, 0.0069 and 0.021 respectively. For 39% WFPS the corresponding values were $p = 0.34$, 0.00076 and 0.018, and for 54% WFPS were $p = 0.022$, 0.00024 and 0.00092.

AFPS) for 1% and 5% biochar composites was significantly greater than for BC100% treatments per unit weight of biochar ($p = 0.044$ and 0.015 respectively). For treatments of 1% biochar this measure of unaccounted N_2O was 8.7 (s.e.m. = 1.7, $n = 3$) times greater than the mean for BC100% treatments, and the comparable ratio for treatments of 5% biochar was 4.0 (s.e.m. = 0.37, $n = 3$).

The time to peak headspace [N_2O] (injected $N_2O)^{-1}$ was determined for each treatment, with some slight decline expected thereafter due to continued sample removal alone. These values (see Supplementary Table S2 online) reflect the trends seen in Fig. 1, namely that the rate of increase in headspace [N_2O] (injected $N_2O)^{-1}$ generally slowed with increase in both biochar content and WFPS. However, the times determined for treatments of medium WFPS, particularly those with 0 and 1% biochar, were somewhat anomalous, being less than the corresponding times for treatments of low WFPS, though not significantly. These differences had parallels in the higher values seen in $\Delta N_2O/inj.N_2O$ for treatments of medium WFPS than the corresponding treatments of low WFPS, though again the differences being of minor significance for treatments of 0, 1 or 5% biochar ($p = 0.33$, 0.062 and 0.075 respectively). The diffusion coefficient of N_2O in water is about four orders of magnitude smaller than in air[3], so increased water content would be expected to retard diffusion. It is surmised that these time-related and headspace [N_2O] effects, though only minor, could have been an artefact related to the repacking of moist soil, possibly leading to creation of some larger channels in the porespace of those soils than in the soils of low WFPS, so allowing a freer passage of injected N_2O to the column headspaces. Any such effect would appear to have been overcome by the higher water content of the corresponding soils with high WFPS, where the mean time to reach peak headspace [N_2O] was greater than for the corresponding drier soils.

There was no increase in headspace [N_2O] detected in the BC100% treatments until 120 min after N_2O injection, and little further increase thereafter (Fig. 1). The mean increase in headspace [N_2O] at tmax in BC100% was only 16.1% of that anticipated from the injected N_2O (Table 1). Amendment of Ferralsol with 5% biochar has been shown to significantly increase soil porosity, pore connectivity and mean pore radius[13]. Each of these changes would be expected to increase the rate of gas diffusion. Yet, for soils of similar WFPS there was no increase in the rate of headspace N_2O accumulation with the

3

addition of biochar. On the contrary, as shown in Fig. 1, the rate of and nett change in headspace $[N_2O]$ (injected $N_2O)^{-1}$ decreased as % biochar and WFPS increased. These significant differences, and the low headspace $[N_2O]$ detected in the BC100% treatments, suggest that adsorption and/or decomposition of injected N_2O is likely to have occurred.

Modelling of N_2O data. Modelling of the effects of N_2O permeation through, and reaction with, a soil sample as a function of WFPS and biochar content can provide insight into the interactions between N_2O, biochar and soil.

To begin, first assume that there is no interaction at all between the N_2O and the soil/biochar composite. Under these conditions the processes being observed in the columns can best be regarded as an effusion experiment, where the N_2O is permeating through the porous structure of the soil/biochar compact as a result of a pressure differential. This process can be modelled based on effusion of gases, which is described by the exponential relationship

$$\Delta N = \Delta N_o \ \exp\left(-\frac{A\overline{v}}{2V}t\right) \tag{1}$$

where ΔN is the number of gas molecules having moved from one side of the porous medium to the other at time t, ΔN_o is the total number of molecules in the system, A is the porous area in the solid composite, $\overline{v}$ is the average speed of the gas molecules, and V is the volume of N_2O gas before effusion starts[22]. Therefore, the process of effusion is exponential in nature. Equation (1) can be adapted to the following form, using the equivalent terms assessed in this study:

$$[N_2O] = A - B \ \exp(-k_1 t) \tag{2}$$

where $[N_2O]$ is the concentration of N_2O in the column headspace, A and B are fitting constants, where A–B is the maximum N_2O concentration change, and k_1 is the rate constant for effusion. Here k_1 is related to the terms in the exponential in the previous expression.

Equations (1) and (2) exclude interactions between the N_2O and the soil/biochar composite through which the N_2O is effusing. Two possible interactions will now be considered: the dissolution of N_2O into the water occupying the pores within the soil/biochar composite, and the reaction of N_2O with the solid components (soil and/or biochar), leading to its decomposition.

The dissolution of N_2O into the water present in the composite can best be considered as a quasi-equilibrium process where the kinetics of dissolution are much faster than any of the other processes ongoing in the chamber. Given the duration of the experiments, this is a realistic assumption. As such, the total amount of gas phase N_2O will be lowered by an amount dictated by the solubility of N_2O in water and the availability of water in the system.

In terms of reaction between the N_2O and soil/biochar composite little is known about the reaction kinetics, in particular the order of the reaction. Therefore, we have assumed that this is a first order process dependent on the partial pressure of gas phase N_2O in the system. That is:

$$[N_2O] = C \ \exp(-k_2 t) \tag{3}$$

where k_2 is the rate constant for decomposition, and C is the initial concentration of N_2O.

Combining all terms together, the resultant expression is:

$$[N_2O] = A - B \ \exp(-k_1 t) - C \ \exp(-k_2 t) \tag{4}$$

This was then fitted to the experimental data using linear least squares regression (see Supplementary Table S4). A good fit was found between the measured headspace $[N_2O]$ values and those predicted from the modelling expression, and there was also a fairly close correspondence of times to peak headspace $[N_2O]$ with those modelled (see Supplementary Table S5). These outcomes offer support to the concepts of diffusion and that adsorption and/or decomposition of injected N_2O is likely to have occurred.

pH and Eh. In the soil/biochar composites pH increased with increases in both soil water and biochar content (Table 2). These changes are consistent with decreased soil $[H^+]$ with increasing water content, and the strong acid-neutralising capacity of the biochar. Values of Eh_{pH7} decreased with increasing WFPS, independent of biochar content, probably due to low oxygen diffusion in water. On the contrary, Eh_{pH7} (Eh corrected to pH = 7) increased with increasing biochar content, most particularly at low WFPS (Table 2). This could lead to the conclusion that biochar addition led to reduction of N_2O, taking electrons from the composite media and thus increasing its redox potential. However, it is unlikely that the small quantity of N_2O injected (22 nmol) would be sufficient to promote such significant changes in ~200 g of composite. Initial rapid mineralisation of biochar C and the priming of mineralisation of native soil organic C following addition of biochar have been observed[23–25]. One or both of these processes, which would be increasingly handicapped by increasing WFPS, would seem to be more likely responsible

Biochar (%)	0			1			5			100
WFPS (%)	12	39	54	12	39	54	12	39	54	6
NH_4^+-N (mg kg^{-1})	24.7 (0.33) a*c****	72.5 (1.50) a*b*	95.3 (0.67) b*c****j*	23.3 (0.33) d***f****	73.0 (1.15) d***e**k*	94.0 (0.00) e**f****n*	24.0 (0.58) g****h**	77.7 (1.20) g***k*	79.7 (3.18) h**j*n*	<0.3
NO_3^--N (mg kg^{-1})	0.2 (0.03) a**b**	1.2 (0.35)	1.9 (0.56)	0.5 (0.01) a**c**	0.9 (0.24)	1.7 (0.26) c**	0.5 (0.01) b**	1.3 (0.51)	0.9 (0.29)	<0.20
pH	5.8 (0) a#b** h#j#	6.0 (0) a#n* q**	6.1 (0.03) b**r* t****	6.1 (0) c*d* h#k#	6.3 (0.03) c*n* p****	6.4 (0.07) d*r*s**	6.7 (0) e**g** j#k#	7.0 (0.03) e**f** p****q**	7.4 (0.03) f**g** s**t****	9.7 (0.1)
Eh_{pH7} (mV)	454 (3.8) a**f* g*h**	382 (7.0) f*	404 (5.8) a**	515 (4.5) b**c** g*j**	405 (6.9) b**	414 (11.6) c**	621 (12.0) d**e*** h**j**	428 (4.0) d**	429 (14.0) e***	499 (13.3)

Table 2. Nitrate- and ammonium-N concentrations, pH and Eh of soil/biochar mixtures after incubation, with Eh values corrected to pH = 7 (s.e.m. in parentheses, $n = 3$). Within rows, means accompanied by the same letter are significantly different ($*p < 0.05$, $**p < 0.01$, $***p < 0.001$, $****p < 0.0001$, #$p = 0$).
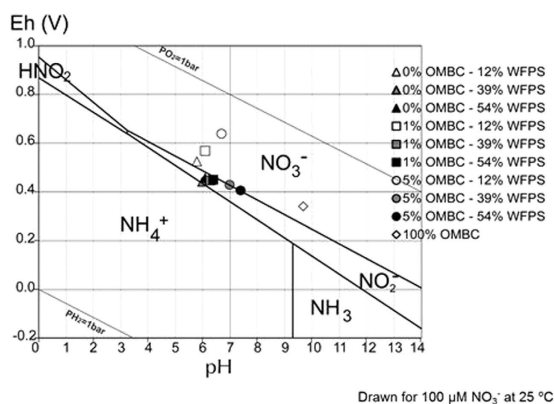

Figure 2. Pourbaix diagram of N representing its various forms in a 100 μM solution at 25 °C as a function of Eh (in V) and pH (diagram drawn using *Medusa software*[60]).

for the changes seen in Eh_{pH7} with increased biochar rate, and would also account for freeing of electrons that might be used in any reduction of N_2O to N_2.

The Pourbaix diagram (Fig. 2) shows that NH_4^+ would not be expected to be the dominant form of N in any of the treatments, and that NO_3^- would dominate, especially in the 5% biochar treatment at low WFPS. Yet this was clearly not the case, with NH_4^+-N dominant in all soil/biochar treatments. Nevertheless, as anticipated, NH_4^+-N increased substantially with increasing WFPS (Table 2). NH_4^+-N, relative to pre-packed soil (44 mg kg^{-1}), had increased in all medium and high WFPS treatments but decreased at low WFPS. In all soils NO_3^--N had decreased markedly (from 23 mg kg^{-1}) to <2 mg kg^{-1} (Table 2). Increased NH_4^+-N would not be likely to result from dissimilatory NO_3^- reduction to NH_4^+, as this is catalysed by bacteria under anaerobic conditions[26]. Likewise, the abiotic reduction of NO_3^- to NH_4^+ involving green rust compounds [$Fe^{II}_4Fe^{III}_2(OH)_{12}SO_4 \cdot yH_2O$], as proposed by Hansen, Koch[27], is also only favoured in anoxic environments. The γ-irradiation of soil has been shown to produce an up to 30-fold increase of NH_4-N_2[28] and up to 100% decrease of NO_3-N_2[29]. This would appear to be the most likely explanation for the changes observed, and the heightened effect of γ-irradiation on NH_4-N with higher soil moisture[30] very strongly supports this conclusion.

X-ray photoelectron spectroscopy. Results of the analysis of the C and N surface functional groups of the unincubated (original non-irradiated biochar without injected N_2O – see Method) and aged biochars are presented in Table 3 and Table 4. There was a substantial change in both the concentration of the C functional groups on the surfaces of the biochar pooled from the low, medium and high WFPS 5% treatments (known as LMH5%) and a smaller reduction on BC100%. For LMH5% the concentration of aromatic/aliphatic C=C/C-C/C-H and shake up peaks are much lower, and the BC100% lower, than for the unincubated biochar. The carboxylic and the C-O content had increased for both treatments compared with the unincubated biochar. However an increase in the C=O groups was only measured in the LMH5%. Carbonates were also detected on the surface of the LMH5% from the soil but not on the unincubated biochar or the BC100% treatment. These findings for the biochar from the soil are consistent with those of[16,31] who measured the oxidation of the surface of the biochar after addition to

	Unincubated biochar			Biochar from LMH5% soils		BC100% after addition of N_2O		
Name	Functional Groups	Peak BE (mV)	At. %	Peak BE (mV)	At. %	Functional Groups	Peak BE (mV)	At. %
C1s A	C=C/C-C/C-H	284.47	68.24	284.38	35.68	C=C/C-C/C-H	284.57	57.10
C1s B	C-O	286.57	6.76			C-O	286.56	12.11
C1s C	C=O	287.97	2.40	286.48	8.04	C=O	287.96	3.35
C1s D	O=C-O	289.17	0.53	287.88	2.89	O=C-O	289.16	3.65
C1s E	Shake up peaks	290.36	6.70	289.08	2.74			
C1s F						Shake up peaks	290.87	4.23
	Carbonate			291.21	1.21			
N1s A	-O-C=N/pyridine pyrrole/NH_3	400.42	0.40	400.47	0.77		400.93	0.49
N1s B	NH_4/NH_2 groups	398.55	0.28	398.69	0.13		399.23	0.25
N1s C	Pyridine/N-O/Chemisorbed NH_3			402.56	0.11			

Table 3. C 1s and N 1s bonding state and their relative atomic percentage on the biochar surfaces of eucalypt biochar before addition to columns, extracted from the soil LMH5% treatments and from the 100% biochar treatment, as determined by XPS (regional scan).

	Unincubated BC		LMH5%		BC100%	
Name	Peak BE	At. %	Peak BE	At. %	Peak BE	At. %
C1s	284.56	82.38	284.63	42.77	285.39	73.72
O1s	532.42	14.39	532.67	39.40	533.16	19.20
Ca2p	348.08	1.84	347.70	0.75	348.66	2.39
Al2p	nd	nd	75.39	7.37	75.63	0.28
Si2p	103.44	0.51	103.78	7.31	103.89	0.97
Fe2p			712.20	1.32		
N1s	400.14	0.88	400.59	1.07	401.60	0.98
S2p					169.70	0.28
P2p					135.02	0.29
K2s					378.63	0.46

Table 4. XPS survey of the C, N, O and mineral elements in the three biochar samples (nd = not detected).

soil. A large increase in the -O-C=N /pyridine pyrrole/NH_3 was measured in the LMH5%, and a much smaller increase in the BC100%, when compared with the unincubated biochar. A new N group for the LMH5% was detected at 402.56 eV which is often associated with the Pyridine/N-O/Chemisorbed ammonia (NH_3) and/or the formation of a conjugated N-C-N configuration[32].

Table 4 reveals considerable differences between the mineral content on the surface of the unincubated biochar and the BC100% and the LMH5%. Iron was present on the surface at 1.3% and silicon (Si) and aluminium (Al) at approximately 7.3% in the LMH5%, whereas no Fe was measured in the unincubated biochar or the BC100%. Silicon and Al were not detected on the surface of the unincubated biochar and only a small amount was detected on the BC100%. Total surface N was increased from approximately 0.9% in the unincubated biochar to 1% in BC100%, and to 1.1% in LMH5%.

Scanning transmission electron and transmission electron microscopy: examination of the surface and internal structure of aged eucalypt biochar.   The structure of the biochar before application to soil is shown in Supplementary Fig. S2. It can be seen that the internal and external C surfaces are typical of a woody biochar that has high C content and a very low mineral content. There were no significant structural or compositional differences noted between the incubated BC100% and the unincubated biochar.

Figure 3 characterises some of the changes that have occurred on the surfaces of the LMH5%. Some of the internal pores have a layer of organic molecules that are rich in Ca and Mg (Fig. 3b: energy dispersive x-ray (EDS)) and some of the pores have filled with organic matter and mineral matter that is high in Al/
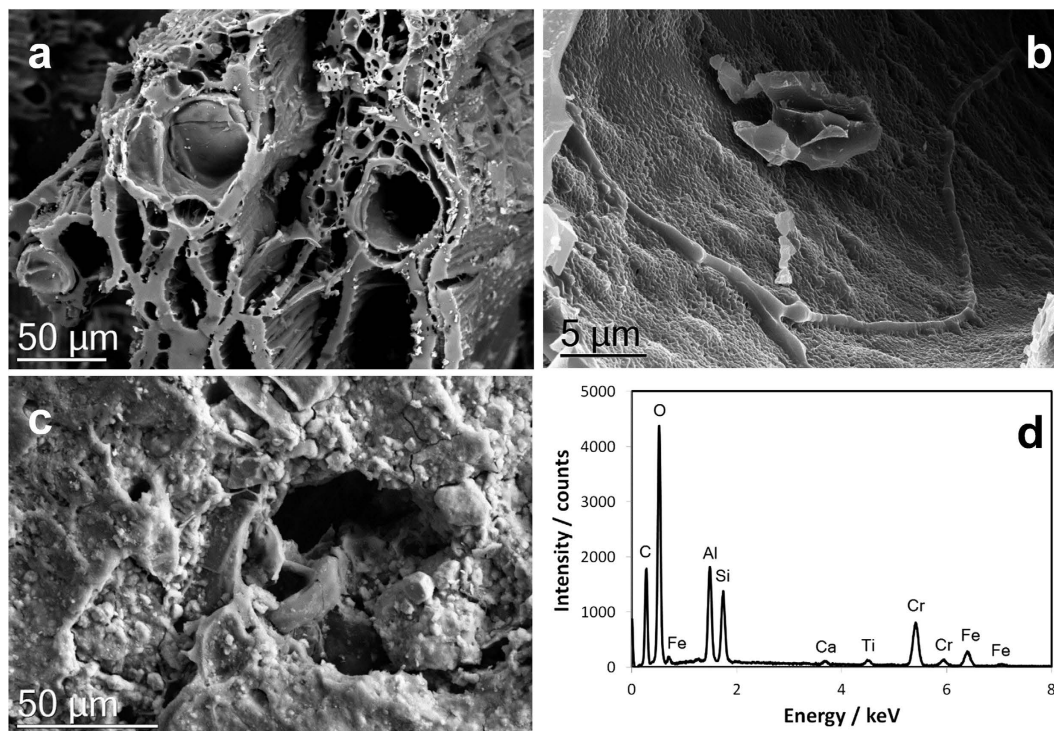
Figure 3. (**a**) SEM image of xylem in the biochar after interaction with soil; (**b**) Internal surfaces of the xylem of the biochar coated in an organomineral film containing significant amounts of Ca and Mg; (**c**) external surface of the biochar and a pore coated with a range of minerals, and (**d**) the EDS spectrum of (**c**).

Si/O, Fe/O /, Ca/C/O and Ti/O compounds (Fig. 3c). Figure 3d illustrates the range of different mineral phases observed on the surface of the biochar. The EDS data mirrors the survey analysis carried out using x-ray photoelectron spectroscopy (XPS).

Scanning transmission electron microscope (STEM) images and x-ray mapping reveal a nanostructure that is highly heterogeneous. Figure 4 shows a high angle annular dark field (HAADF) STEM image of a section of the biochar particle that has interacted with the soil organic and mineral matter. The associated EDS spectra (Fig. 4) demonstrate the considerable organic content of the mineral phases (see also Supplementary Figure S3). Electron energy loss spectrometry (EELS) of the regions showed strong Fe signals but of varying oxidation state (Fig. 5) with some of the Fe/O phases having an oxidation state of $3+$ (haematite) and others a mixed oxidation state of $2+/3+$ (possibly magnetite). Transmission electron microscopy (TEM) imaging with selected area electron diffraction indicated that these nanophases could be a mixture of haematite, magnetite and possibly goethite (see Supplementary Figure S4). Figure 6 is an analysis of another interface between a biochar region and a region that has a number of nanophase minerals. On the biochar boundary there are nanophase particles rich in Si/O (probably SiO_2) and also Fe/O phases that have a mixed (II-III) Fe oxidation state (probably magnetite). In the organomineral phase adjacent to the biochar there are various Al/Si/Ca/Fe/C/S/O nanophase minerals.

Discussion

In columns containing soil/biochar composites and 100% biochar, nett headspace $[N_2O]$ was significantly lowered when N_2O was injected into the profile. This has important consequences for global mitigation options for this greenhouse gas, which also depletes stratospheric ozone[33]. This observation is consistent with studies showing that biochars can lower N_2O emissions from the soil surface[6]. These previous studies have paid little attention to the different mechanisms involved[10,14]. We have shown definitively that that abiotic consumption and/or adsorption of N_2O is an important mechanism in the studied system.

The interception of N_2O was not related to soil/biochar moisture content, in the range approx. 12–54% WFPS. Diminishing N_2O emissions were observed with increasing biochar content in the soil. Cornelissen, Rutherford[17] examined the sorption properties of a range of softwood biochars. Two, with comparable BET surface areas (176 and 286 m^2 g^{-1}) to the eucalypt biochar, had Langmuir maximum sorption capacities for N_2O of 47 and 55 cm^3 g^{-1} respectively at 20 °C under anhydrous conditions, equivalent to 1.95 and 2.29 $mmol$ g^{-1}. The BC100% treatments contained a mean 72.7 g of biochar in a close to anhydrous state. It thus seems highly probable that the apparent 'loss' of 84% of the mean injected 22.2 nmol of N_2O from BC100% treatments (Table 1), as calculated from headspace $[N_2O]$, could be attributed to adsorption. Comparing BC100% with unincubated biochar, there was a small increase from
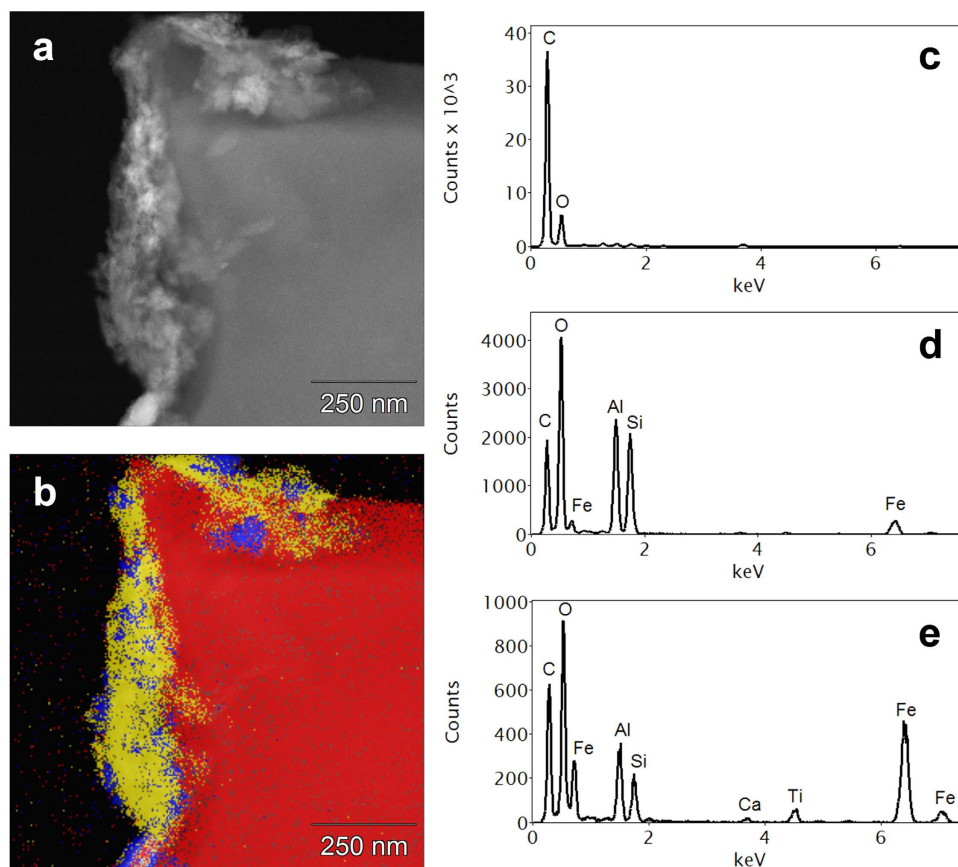
Figure 4. (**a**) HAADF image showing an organomineral layer (bright) coating an external surface of a biochar particle; (**b**) Phase map of (**a**) derived from x-ray microanalysis spectrum imaging, showing three distinct phases; Average EDS spectra of: (**c**) red (biochar) phase in (**b**) containing C and O only; (**d**) yellow (clay) phase in (**b**) containing mainly C, O, Al and Si; (**e**) blue (Fe-rich) phase in (**b**). Both mineral phases [(**c,d**)] have a considerable organic content.
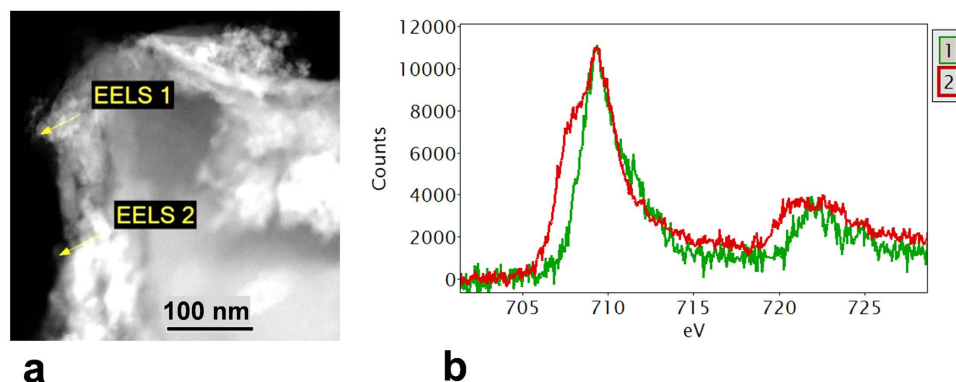
Figure 5. (**a**) STEM HAADF image of biochar with organomineral layer; (**b**) Fe-L$_{2,3}$ EELS spectra (background stripped) were obtained from the points marked in (**a**). The EELS 1 spectrum is characteristic of haematite (Fe III). The spectrum from EELS 2 (red line) shows a pronounced low energy shoulder, suggesting a mixed (II–III) valence state. Note: peak maxima aligned at 709 eV for comparison.

0.40 to 0.49 atom % of -O-C $=$ N/pyridine pyrrole/NH$_3$ revealed by XPS, possibly as a consequence of reaction with (consumption of) N$_2$O. The XPS results of the LMH 5% samples indicated that there had been a considerable increase in the -O-C $=$ N /pyridine pyrrole/NH$_3$, to 0.77 atom %, and appearance of pyridine/N-O/chemisorbed NH$_3$ and/or possibly the formation of a conjugated N-C-N configuration[32] (Table 3). It is apparent from these increases in N-C/H-N –O-C $=$ N groups that N$_2$O had been adsorbed
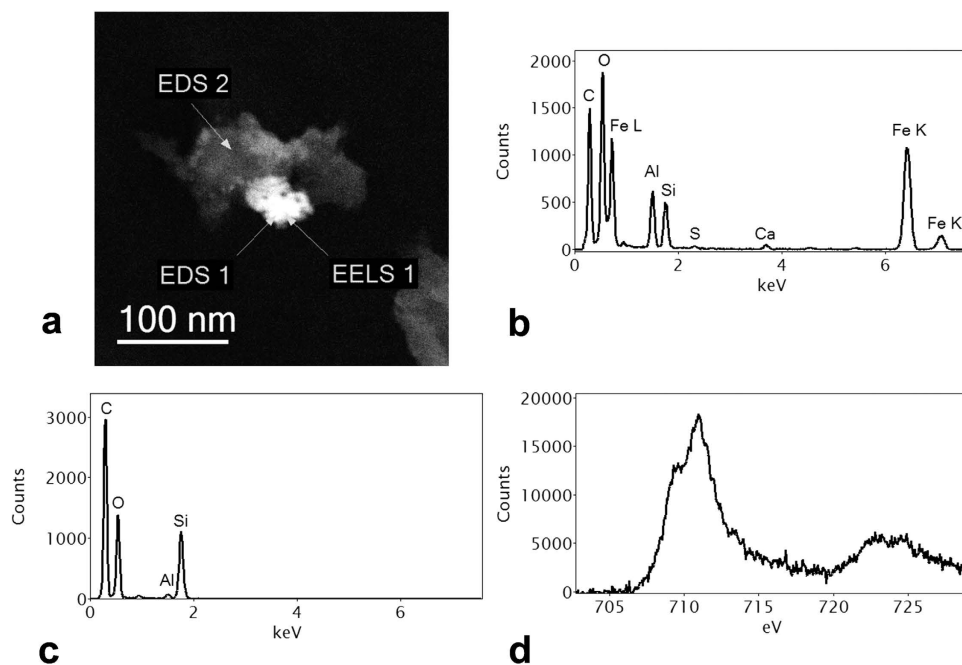
Figure 6. (**a**) STEM HAADF image of edge of biochar showing organomineral phase formed by reaction with soil; (**b**) EDS spectrum of Fe-rich mineral phase (EDS 1); (**c**) EDS spectrum of Si-rich phase (EDS 2); (**d**) Fe-$L_{2,3}$ EELS spectrum (background stripped) at EELS 1 showing a pronounced low energy shoulder on the Fe-L_3 edge at around 708 eV, characteristic of a mixed (Fe II–III) valence state such as found in magnetite.
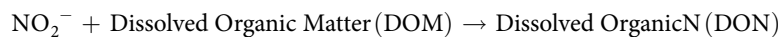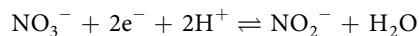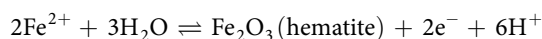
onto the surface of the biochar and could have undergone reactions both with the C and some of the mineral elements (especially Fe nanophase particles identified by TEM) in the biochar. A similar finding re adsorption of N_2O was reported by Cornelissen, Rutherford[17]. The significantly greater unaccounted N_2O per unit weight of biochar from headspace and AFPS in soil/biochar treatments than from BC100% also suggests that additional mechanisms may have been responsible for this loss than for that in the BC100%.

The increase in the COOH content (Table 3) and Fe/Al/Si content (Table 4) of the LMH5% is consistent with the findings of Joseph, Camps Arbestain[16] and Lin, Munroe[34] who measured the changes to poultry manure/sawdust, greenwaste and paper sludge biochars after 2 years, and poultry manure/sawdust and paper sludge biochars after 3 months respectively in the same Ferralsol used in this study. The latter study found biochars in Ferralsol formed oxidised C surfaces and reacted with soil organic matter. The formation of a porous organomineral layer resulting in the appearance of Fe compounds with Fe^{2+}/Fe^{3+} oxidation state indicated that redox reactions[20] between the N_2O and the Fe cations may have taken place.
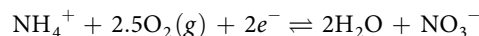
N_2O is a very strong oxidant. It has a standard reduction potential of 1.77 V, which makes it stronger than O_2 (1.23 V) and Fe(III) (0.77 V)[35]. Thus it was expected that the 100% biochar would have acted as a catalytic surface to promote the reduction of N_2O. Our data indicate that biochars will not significantly reduce N_2O without formation of either redox active organic compounds or organomineral phases high in Fe and other transition metals on their surface. This is consistent with the findings of Carabineiro, Fernandes[36] who noted that catalysts are required on the surface of activated C to speed up N_2O reduction reactions at low temperatures.

Reaction of N_2O might occur with either redox active water soluble organic molecules on the surface of the biochar and/or organic molecules that are deposited from the soil as the organomineral layer is formed during the biochar ageing process. Avdeev, Ruzankin[37] reported that a range of aromatic and aliphatic compounds are oxidized by N_2O. They hypothesised that an O atom is transferred through the 1,3-dipolar cyclo-addition of N_2O to the C=C bond with the resulting intermediate decomposing to yield a ketone and N_2. Biochars contain a range of aromatic and non-aromatic compounds on their internal and external surfaces. The XPS data presented here, showing substantial increase in ketonic groups in LMH5% (Table 3), indicate that this reaction has taken place.

It is also consistent with the recent research related to the role of Fe^{2+}/Fe^{3+} cycling, Eh/pH with N release dynamics and formation and reduction of N_2O[38]. It should be noted that the soil contains NH_4^+ and NO_3^- and these can exist in solution within the water filled pores and from there bind to the surfaces of the biochar. With the injection of N_2O the following sequence of reactions could take place.

$$N_2O + 2e^- + 2H^+ \rightleftharpoons N_2 + H_2O$$

$$2Fe^{2+} + 3H_2O \rightleftharpoons Fe_2O_3\,(\text{hematite}) + 2e^- + 6H^+$$

$$NO_3^- + 2e^- + 2H^+ \rightleftharpoons NO_2^- + H_2O$$

$$NO_2^- + \text{Dissolved Organic Matter}\,(\text{DOM}) \rightarrow \text{Dissolved Organic N}\,(\text{DON})$$

(hypothesised by Li, Yu[39])

$$NH_4^+ + 2.5O_2\,(g) + 2e^- \rightleftharpoons 2H_2O + NO_3^-$$

Results of the XPS and the examination of the aged biochar surfaces indicated that there had been significant reactions. Iron has already been reported as a vital key for orchestrating N-transformations[27,40-42]. Li, Yu[39] have shown that reduction and oxidation of N compounds are enhanced when Fe and organic matter are also oxidized or reduced. They refer to this as the "FeIII–FeII redox wheel". A similar mechanism was found in anoxic environments by Klüpfel, Piepenbrock[43]. Reactions between Fe^{2+} and either NO_3^- or NO_2^- to produce N_2 (reduced species) are energetically favourable resulting in the formation of iron (oxy-)hydroxide[40]. The addition of amorphous Fe(III)hydroxide (HFO) and, to a lesser extent magnetite, greatly accelerated rates of reaction compared to systems containing Fe^{2+} alone[40]. If N_2O is adsorbed onto the surfaces of these nanoparticles or if soluble N_2O surrounds the nanoparticles, catalytic reduction of N_2O is likely. Sang, Kim[44] proposed the following reaction mechanism as being the most likely to fit their experimental data for the reduction of N_2O on Fe exchanged zeolites. This reaction mechanism may also be occurring in the organomineral phases and in the pores of the biochars where there is a concentration of nanophase Fe.

$$N_2O + FeO \quad \rightleftharpoons \quad N_2O - FeO \tag{A}$$

$$N_2O - FeO \quad \rightleftharpoons \quad OFeO + N_2 \tag{B}$$

$$N_2O + OFeO \quad \rightleftharpoons \quad N_2O - OFeO \tag{C}$$

$$N_2O - OFeO \quad \rightleftharpoons \quad O_2 - FeO + N_2 \tag{D}$$

$$O_2 - FeO \quad \rightleftharpoons \quad FeO + O_2 \tag{E}$$
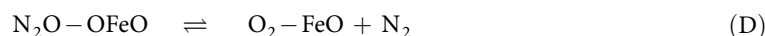
It is true that the system used in this study was not natural, lacking biological activity. Nonetheless, there have been numerous studies investigating the influence of biochar on biological aspects associated with changes to N_2O emissions from soil, and not all of these changes could be easily explained and indeed, the importance of abiotic reactions has been highlighted in numerous works, e.g. Van Zwieten, Kammann[11], and Cayuela, Sánchez-Monedero[18]. This work was designed to investigate abiotic reactions following a moderate degree of aging between the biochar and the soil. There is no information on the impact of γ-irradiation on biochar, so this may have impacted the results obtained showing biochar retarded N_2O movement through the soil profile. However, we deemed it necessary to sterilise the matrix in this way, as other methods (i.e. autoclaving, oven, etc.) could be equally influential in changing properties of biochar.

In summation, eucalypt biochar was shown to lower emissions of injected N_2O via abiotic mechanisms. In the 100% biochar treatment, the decline in $[N_2O]$ may be solely the result of adsorption. Given the small quantities of N_2O injected this could explain why the nett N_2O in the headspace is substantially less for the 100% biochar than for the soil/biochar treatments, or indeed the sand column system control. The significantly greater decline seen in the composite treatments per unit of biochar, combined with the changes revealed by XPS in biochar from the 5% treatments and changes in Eh_{pH7}, suggest very strongly that redox reactions have occurred, reducing a proportion of the intercepted N_2O to N_2. There remains much to understand about the importance of abiotic and redox properties in altering soil GHG emissions following biochar addition, yet this offers a significant opportunity to address a globally important issue.

Materials and Methods

Soil and Biochar. A Ferralsol[45] from Wollongbar (28º50'S, 153º25'E) in north-eastern New South Wales was sieved to ≤2 mm. The soil was rich in Fe sesquioxides (clay content 44.1%; total organic C 4.39%)[46], with total Fe 8.4%, total Mn 350 mg kg^{-1}, total C 4.9%, total N 0.47% and pH of 4.2 in CaCl$_2$[47], NH_4^+-N and NO_3^--N contents of 44 and 23 mg kg^{-1} respectively, with NO_2^--N < 0.10 mg kg^{-1}

(analytical laboratory accredited to ISO17025). Biochar was obtained from Pacific Pyrolysis, made from the woody residue of *Eucalyptus polybractea* after steam extraction of eucalypt oil. It was produced using a semi-continuous 40 kg h^{-1} pilot unit at a highest treatment temperature (HTT) of 550 °C and heating rate of 5–10 °C min^{-1}. Residence time at HTT was 45 min. Measured prior to application the biochar had a pH of 8.65 in CaCl$_2$, an acid neutralising capacity of 8.8 (%CaCO$_3$ eq.), electrical conductivity of 1.5 dS m^{-1}, total C of 70% and total N of 0.81%, NH$_4^+$-N and NO$_3^-$-N contents of 0.49 and <0.2 mg kg^{-1} respectively, Fe content of 0.24% and Mn of 300 mg kg^{-1}, and CEC of 17 cmol($^+$)/kg C[48], a molar H:C$_{org}$ ratio of 0.48 and BET specific surface area of 269 m^2 g^{-1} [46]. The ash content was 11.6%, containing 9,900 and 5,400 mg kg^{-1} of Fe and Mn respectively[49]. (All chemical properties determined by ultimate and proximate analysis using the Australian Standard methods AS 1038.5, AS 1038.6.1 and AS 1038.3).

Sample packing and irradiation. Air dried soil was sieved to ≤2 mm and biochar to between 250 μm and 2 mm to enhance homogeneity of mixing into small soil volumes. Biochar dosing rates into the columns were 0, 1, 5 and 100% (w/w, dry) biochar, while a system (method check) control of acid-washed sand was also utilized. The columns were 300 mm tall PVC tubes of 37 mm internal diameter, fitted with airtight base and top caps. Each column had a sampling port in the top cap and an injection port in the base cap comprising butyl rubber septa (see Supplementary Figure S1). Soil and soil/biochar mixtures were repacked in 3 equal sections to a depth of 200 mm. Components for each section were individually weighed and distilled water added (by weight) during mixing to homogeneity for the three levels of soil moisture, being 12, 39 and 54% WFPS ($n=3$) (see Supplementary Table S1 online). Unamended soils were repacked to field bulk density (BD) of 1.02 g cm^{-3}. Composites of 1 and 5% biochar were repacked to BDs of 1.00 and 0.93 g cm^{-3} respectively, to account for the lower BD of the biochar (see Supplementary Method online). Columns of 100% biochar and system controls of acid-washed sand were both repacked using gentle tapping (neither with additional moisture) to respective BDs of 0.34 and 1.65 g cm^{-3} ($n=3$).

The porosities of the soil, 1 and 5% biochar composites and sand were 61.5, 61.9, 63.4 and 37.7% respectively, and that of the biochar from its BD and the density of its solid C fraction[50] to be between 75 and 80% (see Supplementary Method online). The WFPS of each set of replicate columns was determined as the volumetric water content (see Supplementary Table S1) divided by the relevant porosity.

After repacking, a muslin covered non-absorbent cotton wool plug was inserted into the top of each column to secure the test matrix, and top caps fitted and sealed, enabling the columns to be shipped in an upright position without any disturbance of the packed contents. All columns were weighed and γ-irradiated, using a minimum dose of 25 kGy in order to render the contents abiotic[51,52]. The packing was removed from each column inside a UV sterilized biological safety cabinet and the column resealed in the same abiotic environment. Each column was then re-weighed to determine any loss in moisture (none detected). The columns were then incubated at 23 °C for 4 months before N$_2$O injection. They were later tested for biological activity (see below). At all stages care was taken to avoid disturbance of the contents.

Injection of N$_2$O and headspace sampling. Injection mixtures (IMs) of N$_2$O (>99.8% pure) diluted in N$_2$ (99.999% pure) were prepared in 500 mL Tedlar® bags. Samples ($n=3$) of each IM were injected into pre-evacuated 12 mL Exetainer® vials for later analysis. A 2 mL sample of the IM was injected through the base port using a gas-tight glass syringe with Teflon plunger and a 23G × 1¼" needle inserted to be centre of the column. Immediately prior to injection, and at specific post-injection intervals (see Supplementary Table S3), 2 mL samples of headspace gas were withdrawn through the top port. A tap connected through a side port immediately above the column contents (see Supplementary Figure S1) was opened only during sample withdrawals to maintain atmospheric pressure in the headspace.

Gas samples were analysed according to Van Zwieten, Kimber[47] (see also Supplementary Method). The rate of diffusion and any abiotic adsorption or degradation of N$_2$O gas injected at the base was measured by its accumulation in the column headspace. Pre-injection headspace [N$_2$O] was assumed to be in equilibrium with that of air-filled pore space (AFPS [%] = 100 - WFPS), itself assumed to be in equilibrium with N$_2$O dissolved in WFPS. From headspace [N$_2$O] an estimate was made of the quantity of N$_2$O dissolved in WFPS (see Supplementary Method). Total gas pressure within both the headspace of the columns and soil air was assumed to be atmospheric. Dissolved N$_2$O was assumed to be in equilibrium with N$_2$O in AFPS at the time corresponding to maximum headspace [N$_2$O]. For each column the total quantity of N$_2$O in headspace, AFPS and WFPS prior to injection was deducted from the same total at diffusive equilibrium, the difference being divided by the quantity of N$_2$O injected.

At the end of the experiment, 3 g of substrate was carefully removed from the upper surface of the columns, within the biological safety cabinet, and the columns resealed (see Supplementary Method). These samples were analysed for microbial activity by fluorescein diacetate (FDA) hydrolysis[53]. A range of 0.17–0.34 μg sodium fluorescein (g dry matrix)$^{-1}$ min^{-1} confirmed insignificant microbial activity. The small quantity detected may have resulted from residual enzyme activity[54].

pH and Eh. All soil/biochar composites and the BC100% were analysed at the completion of the incubation and gas sampling for NH$_4^+$-N and NO$_3^-$-N content, pH (in H$_2$O) by the method of[55], and redox

potential (Eh)[56] using a hand held ORP meter (Hanna HI 98160) with platinum electrode (Table 2). Redox potentials were transformed[57,58] to correct the Eh to pH = 7 (Eh$_{pH7}$), referenced to the standard hydrogen electrode through the following equation:

$$Eh_{pH7} = Eh - \frac{RT}{F} \times \ln 10 \times (7 - pH)$$

(5)

where R is the ideal gas constant (8.31447 J K^{-1} mol^{-1}), F the Faraday constant (96485.34 C mol^{-1}), and T the temperature (in K).

All Eh measurements were recorded at 25 °C, where

$Eh_{pH7} = Eh - 0.059 (7 - pH)$, with Eh expressed in V.

Examination of the biochar after adsorption of N$_2$O. To help determine the possible mechanisms that resulted in the reduction in N$_2$O, biochar was studied using a range of electron microscopy and x-ray photoelectron spectroscopy (XPS) techniques. Biochar pieces from different water content columns using the 5% soil/biochar matrix were separated[16,34] and crushed to pass a 0.1mm sieve. Representative samples of the BC100% treatments, and the unincubated biochar (original non-irradiated biochar stored frozen in a sealed container and without injected N$_2$O), were also crushed and sieved. Surface functional groups and major mineral elements of the unincubated biochar, the biochar extracted from the soil and the BC100% treatment were measured by XPS analysis (Thermo Scientific ESCALAB250Xi), using a 500 micron diameter beam of monochromatic Al-Kα radiation (photon energy = 1486.6 eV) at a pass energy of 20 eV. The core level binding energies (BEs) were aligned with respect to the C1s BE of 285.0 eV. Examination of over 50 biochar pieces was carried out using a Zeiss Sigma scanning electron microscope (SEM) fitted with a Bruker energy dispersive x-ray analyser as described in Joseph, Graber[59]. To provide detailed microstructural, crystallographic and microchemical analysis both transmission electron microscopy (TEM) and scanning transmission electron microscopy (SEM) was undertaken using JEOL ARM200F aberration corrected TEM fitted with an electron energy loss spectrometer and JEOL EDS detector. To help determine the crystal structure of the mineral phases selected area electron diffraction was carried out in TEM mode (see Supplementary Method for further details of sample preparation and conditions of both TEM and SEM examination).

Statistical analysis. All statistical comparisons of two groups of data used a two-tailed Welch's t-test, on account of its suitability for mean values with unequal variance. Unless otherwise stated, any significant difference is based on a 95% confidence level.

References

1. Butterbach-Bahl K., Baggs E. M., Dannenmann M., Kiese R. & Zechmeister-Boltenstern S. Nitrous oxide emissions from soils: how well do we understand the processes and their controls? *Philos. T. Roy. Soc. B* **368,** 1621, doi: 10.1098/rstb.2013.0122 (2013).
2. Clough T. J., Sherlock R. R. & Rolston D. E. A Review of the Movement and Fate of N$_2$O in the Subsoil. *Nutr. Cycl. Agroecosyst.* **72,** 3–11 (2005).
3. Heincke M. & Kaupenjohann M. Effects of soil solution on the dynamics of N$_2$O emissions: a review. *Nutr. Cycl. Agroecosyst.* **55,** 133–157 (1999).
4. Mukherjee A. & Lal R. The biochar dilemma. *Soil Res.* **52,** 217–230 (2014).
5. Sánchez-García M., Roig A., Sanchez-Monedero M. A. & Cayuela M. L. Biochar increases soil N$_2$O emissions produced by nitrification-mediated pathways. *Front. Environ. Sci.* **2,** 25, doi: 10.3389/fenvs.2014.00025 (2014).
6. Cayuela M. L. *et al.* Biochar's role in mitigating soil nitrous oxide emissions: A review and meta-analysis. *Agr. Ecosyst. Environ.* **191,** 5–16 (2014).
7. Cayuela M. L., Jeffery S. & Van Zwieten L. The molar H:C$_{org}$ ratio of biochar is a key factor in mitigating N$_2$O emissions from soil. *Agr. Ecosyst. Environ.* **202,** 135–138 (2015).
8. Lin X. *et al.* Assessing Microbial Contributions to N$_2$O Impacts Following Biochar Additions. *Agron.* **4,** 478–496 (2014).
9. Davidson E. A., Chorover J. & Dail D. B. A mechanism of abiotic immobilization of nitrate in forest ecosystems: the ferrous wheel hypothesis. *Global Change. Biol.* **9,** 228–236 (2003).
10. Clough T. J., Condron L. M., Kamman C. & Müller C. A Review of Biochar and Soil Nitrogen Dynamics. *Agron* **3,** 275–293 (2013).
11. Van Zwieten L., *et al.* In *Biochar for Environmental Management: Science, Technology and Implementation* 2nd edn (eds Lehmann J., Joseph S.) Ch. 17, 489–520 Routledge (2015).
12. Shcherbak I. & Robertson G. P. Determining the Diffusivity of Nitrous Oxide in Soil using *In Situ* Tracers. *Soil Sci. Soc. Am. J. J* **78,** 79–88 (2014).
13. Quin P. R. *et al.* Oil mallee biochar improves soil structural properties—A study with x-ray micro-CT. *Agr. Ecosyst. Environ.* **191,** 142–149 (2014).
14. Sun Z. *et al.* Direct and Indirect Short-term Effects of Biochar on Physical Characteristics of an Arable Sandy Loam. *Soil Sci.* **178,** 465–473 (2013).
15. Harter J. *et al.* Linking N$_2$O emissions from biochar-amended soil to the structure and function of the N-cycling microbial community. *ISME J.* **8,** 660–674 (2014).
16. Joseph S. D. *et al.* An investigation into the reactions of biochar in soil. *Aust. J. Soil Res.* **48,** 501–515 (2010).
17. Cornelissen G. *et al.* Sorption of Pure N$_2$O to Biochars and Other Organic and Inorganic Materials under Anhydrous Conditions. *Environ. Sci. Technol.* **47,** 7704–7712 (2013).
18. Cayuela M. L. *et al.* Biochar and denitrification in soils: when, how much and why does biochar reduce N$_2$O emissions? *Sci. Rep.* **3,** 1732, doi: 10.1038/srep01732 (2013).
19. Klüpfel L., Keiluweit M., Kleber M. & Sander M. Redox Properties of Plant Biomass-Derived Black Carbon (Biochar). *Environ. Sci. Technol.* **48,** 5601–5611 (2014).

20. Joseph S. *et al.* The Electrochemical Properties of Biochars and How They Affect Soil Redox Properties and Processes. *Agron.* **5,** 322 (2015).
21. Melton E. D., Swanner E. D., Behrens S., Schmidt C. & Kappler A. The interplay of microbially mediated and abiotic reactions in the biogeochemical Fe cycle. *Nat. Rev. Micro.* **12,** 797–808 (2014).
22. Hirsch W. & Fried V. Gas effusion - A relaxation process. *J. Chem. Educ.* **57 (10),** 706 (1980).
23. Zimmerman A. R., Gao B. & Ahn M.-Y. Positive and negative carbon mineralization priming effects among a variety of biochar-amended soils. *Soil. Biol. Biochem.* **43,** 1169–1179 (2011).
24. Luo Y., Durenkamp M., De Nobili M., Lin Q. & Brookes P. C. Short term soil priming effects and the mineralisation of biochar following its incorporation to soils of different pH. *Soil. Biol. Biochem.* **43,** 2304–2314 (2011).
25. Fang Y., Singh B. P. & Singh B. Temperature sensitivity of biochar and native carbon mineralisation in biochar-amended soils. *Agr. Ecosyst. Environ.* **191,** 158–167 (2014).
26. Butterbach-Bahl K., *et al.* In *The European Nitrogen Assessment: Sources, Effects and Policy Perspectives* (eds. Sutton M., *et al.*) Ch. 6, 99–125 Cambridge University Press (2011).
27. Hansen H. C. B., Koch C. B., Nancke-Krogh H., Borggaard O. K. & Sørensen J. Abiotic Nitrate Reduction to Ammonium: Key Role of Green Rust. *Environ. Sci. Technol.* **30,** 2053–2056 (1996).
28. Ramsay A. J. & Bawden A. D. Effects of sterilization and storage on respiration, nitrogen status and direct counts of soil bacteria using acridine orange. *Soil. Biol. Biochem.* **15,** 263–268 (1983).
29. Singh B. R. & Kanehiro Y. Effects of gamma irradiation on the available nitrogen status of soils. *J. Sci. Food Agr.* **21,** 61–64 (1970).
30. McNamara N. P., Black H. I. J., Beresford N. A. & Parekh N. R. Effects of acute gamma irradiation on chemical, physical and biological properties of soils. *Appl. Soil. Ecol.* **24,** 117–132 (2003).
31. Cheng C.-H., Lehmann J., Thies J. E., Burton S. D. & Engelhard M. H. Oxidation of black carbon by biotic and abiotic processes. *Org. Geochem.* **37,** 1477–1488 (2006).
32. Point S., Minea T., Bouchet-Fabre B., Granier A. & Turban G. XPS and NEXAFS characterisation of plasma deposited vertically aligned N-doped MWCNT. *Diam. Relat. Mater.* **14,** 891–895 (2005).
33. Ravishankara A. R., Daniel J. S. & Portmann R. W. Nitrous Oxide (N_2O): The Dominant Ozone-Depleting Substance Emitted in the 21st Century. *Science* **326,** 123–125 (2009).
34. Lin Y., Munroe P., Joseph S., Kimber S. & Van Zwieten L. Nanoscale organo-mineral reactions of biochars in ferrosol: an investigation using microscopy. *Plant Soil* **357,** 369–380 (2012).
35. Aylward G. H., Findlay TJV. *SI Chemical Data*, 5th edn, John Wiley & Sons Australia (2002).
36. Carabineiro S. A. *et al.* N_2O reduction by activated carbon over iron bimetallic catalysts. *Catal. Today* **133–135,** 441–447 (2008).
37. Avdeev V. I., Ruzankin S. F. & Zhidomirov G. M. Molecular mechanism of direct alkene oxidation with nitrous oxide: DFT analysis. *Kinet. Catal.* **46,** 177–188 (2005).
38. Husson O. Redox potential (Eh) and pH as drivers of soil/plant/microorganism systems: a transdisciplinary overview pointing to integrative opportunities for agronomy. *Plant Soil* **362,** 389–417 (2013).
39. Li Y., Yu S., Strong J. & Wang H. Are the biogeochemical cycles of carbon, nitrogen, sulfur, and phosphorus driven by the "FeIII–FeII redox wheel" in dynamic redox environments? *J. Soils Sediments* **12,** 683–693 (2012).
40. Chao T.-T. & Kroontje W. Inorganic Nitrogen Transformations Through the Oxidation and Reduction of Iron1. *Soil. Sci. Soc. Am. J.* **30,** 193–196 (1966).
41. Alowitz M. J. & Scherer M. M. Kinetics of Nitrate, Nitrite, and Cr(VI) Reduction by Iron Metal. *Environ. Sci. Technol.* **36,** 299–306 (2002).
42. Dhakal P., Matocha C. J., Huggins F. E. & Vandiviere M. M. Nitrite Reactivity with Magnetite. *Environ. Sci. Technol.* **47,** 6206–6213 (2013).
43. Klüpfel L., Piepenbrock A., Kappler A. & Sander M. Humic substances as fully regenerable electron acceptors in recurrently anoxic environments. *Nat. Geosci.* **7,** 195–200 (2014).
44. Sang C., Kim B. H. & Lund C. R. F. Effect of NO upon N_2O Decomposition over Fe/ZSM-5 with Low Iron Loading†. *J. Phys. Chem. B* **109,** 2295–2301 (2005).
45. International Union of Soil Sciences Working Group. *World reference base for soil resources 2006: A framework for international classification, correlation and communication.* FAO (2006).
46. Krull E. S. *et al.* From Source to Sink: A National Initiative for Biochar Research. Department of Agriculture. Fisheries and Forestry, Australia (2012).
47. Van Zwieten L. *et al.* Influence of biochars on flux of N_2O and CO_2 from Ferrosol. *Aust. J. Soil Res.* **48,** 555–568 (2010).
48. Rangott G. *Char Analysis Report. Diagnostic and Analytical Services Environmental Laboratory.* Department of Primary Industry (2010).
49. Hunt C. *Char Analysis Report-Ash. Diagnostic and Analytical Services Environmental Laboratory.* Department of Primary Industry (2015).
50. Downie A., Crosky A. & Munroe P. In *Biochar for Environmental Management: Science and Technology* (eds Lehmann J., Joseph S.) Ch. 2, 13–32 Earthscan (2009).
51. Daly M. J., *et al.* Accumulation of Mn(II) in, Deinococcus radiodurans facilitates gamma-radiation resistance. *Science* **306,** 1025–1028 (2004).
52. van Gerwen S. J. C., Rombouts F. M., Van't Riet K. & Zwietering M. H. A data analysis of the irradiation parameter D-10 for bacteria and spores under various conditions. *J. Food Protect.* **62,** 1024–1032 (1999).
53. Zelles L. *et al.* Microbial activity measured in soils stored under different temperature and humidity conditions. *Soil. Biol. Biochem.* **23,** 955–962 (1991).
54. Clarke J. M., Gillings M. R., Altavilla N. & Beattie A. J. Potential problems with fluorescein diacetate assays of cell viability when testing natural products for antimicrobial activity. *J. Microbiol. Meth.* **46,** 261–267 (2001).
55. Rayment G. E. & Lyons D. J. *Soil Chemical Methods - Australasia.* CSIRO Publishing (2010).
56. Fiedler S., Vepraskas M. J. & Richardson J. L. Soil Redox Potential: Importance, Field Measurements, and Observations. *Adv. Agron.* **94,** 1–54 (2007).
57. Glinski J. & Stępniewski W. *Soil aeration and its role for plant*s. CRC Press (1985).
58. Pidello A. Environmental Redox Potential and Redox Capacity Concepts Using a Simple Polarographic Experiment. *J. Chem. Educ.* **80,** 68 (2003).
59. Joseph S., *et al.* Shifting paradigms: development of high-efficiency biochar fertilizers based on nano-structures and soluble components. *Carbon Manag.* **4,** 323–343 (2013).
60. Puigdomenech, I. (2009–2011) Medusa software, available at: https://sites.google.com/site/chemdiagr/ (Accessed: 17th June 2015).

Acknowledgements

Author Contributions

P.Q., S.J. and L.V.Z. conducted principal research. P.Q., S.J., O.H. and S.D. wrote the main manuscript text with assistance from L.V.Z., D.M. and A.C. Figures were prepared by P.Q., S.J., O.H., D.M., P.M. and D.P. All authors reviewed the manuscript.

Additional Information

Supplementary information accompanies this paper at http://www.nature.com/srep

Competing financial interests: The authors declare no competing financial interests.

How to cite this article: Quin, P. *et al.* Lowering N_2O emissions from soils using eucalypt biochar: the importance of redox reactions. *Sci. Rep.* **5**, 16773; doi: 10.1038/srep16773 (2015).